ACS OMEGA

http://pubs.acs.org/journal/acsodf

Article

Multiple-Streams Focusing-Based Cell Separation in High Viscoelasticity Flow

Haidong Feng,* Dhruv Patel, Jules J. Magda, Sage Geher, Paul A. Sigala, and Bruce K. Gale*

Cite This: *ACS Omega* 2022, 7, 41759−41767

Read Online

ACCESS | Metrics & More | Article Recommendations | Supporting Information

ABSTRACT: Viscoelastic flow has been widely used in microfluidic particle separation processes, in which particles get focused on the channel center in diluted viscoelastic flow. In this paper, the transition from single-stream focusing to multiple-streams focusing (MSF) in high viscoelastic flow is observed, which is applied for cell separation processes. Particle focusing stream bifurcation is caused by the balance between elastic force and viscoelastic secondary flow drag force. The influence of cell physical properties, such as cell dimension, shape, and deformability, on the formation of multiple-streams focusing is studied in detail. Particle separation is realized utilizing different separation criteria. The size-based separation of red (RBC) and white (WBC) blood cells is demonstrated in which cells get focused in different streams based on their dimension difference. Cells with different deformabilities get stretched in the viscoelastic flow, leading to the change of focusing streams, and this property is harnessed to separate red blood cells infected with the malaria parasite, *Plasmodium falciparum*. The achieved results promote our understanding of particle movement in the high viscoelastic flow and enable new particle manipulation and separation processes for sample treatment in biofluids.

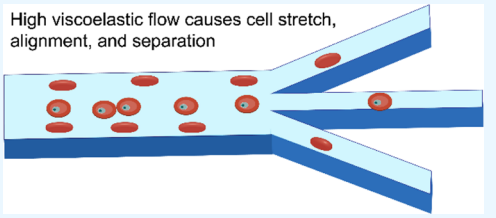

INTRODUCTION

Manipulation and separation of bioparticles are crucial aims in the development of microfluidic devices in biomedical applications. Continuous particle separation has been achieved by manipulating particle movement trajectories, which can be performed by active or passive approaches.[1] In the active particle separation process, a force field is applied to guide particle movement based on different separation criteria.[1,2] In the passive particle separation process, particle flow and particle structure interactions are designed for size- and shape-based separation processes.[1,2] Active separation methods suffer from the requirement of bulk supportive equipment, whereas passive separation methods are limited by problems of high pressure drops and low throughput.[1]

In recent years, hydrodynamic forces have been increasingly utilized to manipulate particle motion.[3−6] The hydrodynamic force-induced particle separation provides a high throughput separation process with a simple device design, which has been applied for bioparticle separation processes such as blood cell separation,[7] circulating tumor cell isolation,[8,9] and sperm retrieval.[10,11] The inertial effect has been proposed to induce particle separation in Newtonian flow[12] and is applied for biosample treatment,[13−15] while particle manipulation and separation in viscoelastic fluid have drawn increasing attention since biofluids with high-concentration biomolecules, such as blood,[16] semen,[17] and DNA solution,[18,19] have viscoelastic properties. The understanding of particle movement in viscoelastic flow contributes to the biofluid treatment process.

In viscoelastic flow, the nonlinear distribution of normal stress differences leads to particle migration toward a low shear stress region.[5,20] Utilizing this phenomenon, size-based particle separation is realized by selectively focusing particles in the channel center.[21] In many cases, viscoelastic flow is combined with other factors, such as inertial flow,[21−24] Dean flow,[25] and the coflow of a Newtonian fluid,[26,27] for the tuning of particle focusing positions and improvement of separation efficiency. However, most of the existing studies explore the viscoelastic focusing phenomenon in a diluted system, in which the first normal stress difference (N_1) dominates particle movement. The influence of the second normal stress difference (N_2) is neglected.[5,28] Biosamples with complex composition and high molecular weight proteins, such as semen and DNA solution, are semidiluted systems at their normal concentration due to molecular entanglement, and cells have different movement trajectories. The understanding of cell movement behavior in semidiluted viscoelastic flow is necessary for cell separation in such a high-concentration biofluid.

In a semidiluted system, N_2 induces a secondary flow in the channel cross section, which influences particle distribution. The secondary flow drag force pushes the particle toward channel sidewalls, which is verified through experiments and numerical simulation.[29,30] The transition from N_1-dominated

Received: September 17, 2022
Accepted: October 25, 2022
Published: November 2, 2022

single-stream focusing to N_2-dominated multiple-streams focusing is observed in a semidiluted polymeric solution with the increase in the flow rate.[31,32] However, the influence of N_2 on particle movement is only estimated using rigid spherical particles in previous studies. Compared to synthetic polystyrene beads, cell movement in high viscoelastic flow is more complex as the cell's physical properties, including dimension, deformability, and shape, will affect cell-flow interaction and cell distribution.

In this paper, cell separation utilizing viscoelastic secondary flow in a high viscoelastic flow is demonstrated. Experiments are performed in a microchannel with a rectangular cross-section utilizing poly(ethylene oxide) (PEO) solution, in which the movement of spherical polystyrene beads, red and white blood cells, and *Plasmodium falciparum* parasite-infected red blood cells is studied. Cells have the transition from single-stream focusing to multiple-streams focusing (MSF) due to the presence of a viscoelastic secondary flow. The cell focusing position is affected by multiple cell physical properties, such as cell dimension, shape, and deformability, which can serve as separation criteria in high viscoelasticity flow.

THEORY

In a confined channel, particle lateral movement in viscoelastic flow is driven by the elastic force F_E. F_E is generated due to the nonlinear distribution of normal stress differences in the channel cross section. In a diluted solution, N_2 has a small magnitude compared to N_1, and its influence on particle movement is neglected.[5,33] Equation 1 shows the estimation of F_E based on N_1 and particle diameter a, where y represents the velocity gradient direction. F_E is influenced by the particle dimension, flow viscoelasticity, and shear rate, and has a direction toward a low shear rate region.[5,34] In the channel with a rectangular cross section, particles migrate to the channel center under the influence of F_E.

$$F_E \sim a^3 \frac{\partial N_1(\gamma)}{\partial(y)} \sim 8a^3\lambda\left(\frac{U}{h}\right)^3 \quad (1)$$

where a is the radius of the particle, γ is the relaxation time, U is the flow velocity, and h is the channel height.

In a high-concentration polymer solution, the increase in N_2 changes fluid flow and the particle focusing position. Polymer molecule entanglement in a semidiluted solution leads to the change of solution viscoelastic properties and the shear thinning phenomenon.[35] In the entangled polymer solution, the magnitude of both N_1 and N_2 increases with the increase in the shear rate, while the ratio of N_2 to N_1 increases up to 30%.[36] N_2 has a direct influence on fluid flow in the lateral direction and induces a viscoelastic secondary flow.[37−39] In a rectangular channel cross section, asymmetric vortex pairs appear,[38] as shown in Figure 1a. The drag force induced by viscoelastic secondary flow F_{SFD} causes particle lateral movement and changes particle focusing positions. F_{SFD} is estimated by Stokes' drag force using the secondary flow velocity V_{SF}.[30]

$$F_{SFD} \sim 3\pi\eta a V_{SF} \sim 3\pi\eta a\left(\lambda Z\frac{U}{2D_h}\right)^4 \quad (2)$$

where η is the fluid viscosity and Z is a constant that depends on the channel aspect ratio $AR = w/h$.

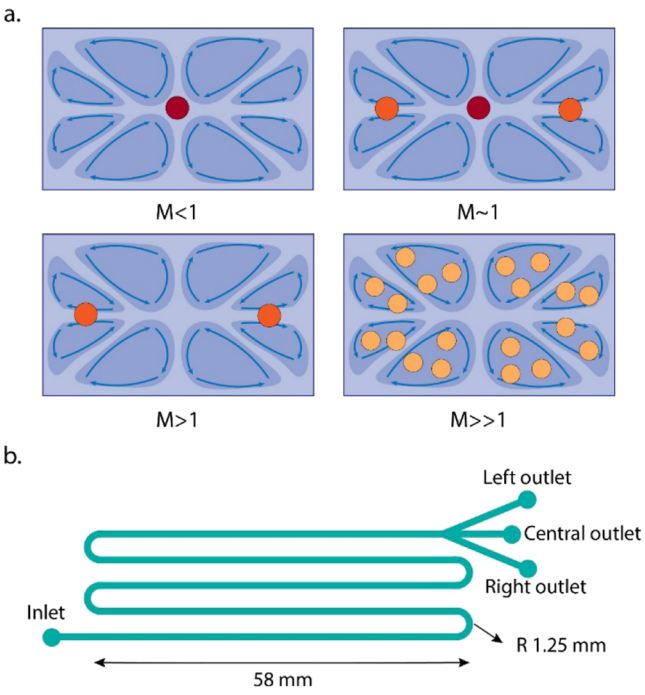

Figure 1. Multiple-streams focusing mechanism and the channel setup. (a) Particle distribution in the channel cross section with different M. (b) Diagram of the microfluidic channel design used in this study. The channel cross section is 150 μm × 50 μm, and the total channel length is 300 mm.

Particle movement in high viscoelastic flow is affected by both F_E and F_{SFD}, as F_E pushes particles toward the channel center, while F_{SFD} leads to particles trapping in secondary flow vortices. The influence of F_E and F_{SFD} on particle movement can be characterized by a ratio M, as shown in eq 3.

$$M = \frac{F_{SFD}}{F_E} = \frac{3\pi\eta Z^4 U\lambda^3 h^3}{128a^2{D_h}^4} \quad (3)$$

Particle focusing positions are determined by M, as shown in Figure 1a. When $M < 1$, F_E dominates particle movement, and particles get focused on the channel center line. When $M \sim 1$, F_E is balanced with F_{SFD}, and particles get pulled out from the central focusing position. In the rectangular channel cross section, the shear stress gradient is smaller in the channel width direction compared to the channel height direction. As a result, F_{SFD} is balanced with F_E in the channel width direction. Particles start to move away from the channel center, and two new focusing positions are formed under the balance between F_E, F_{SFD}, and wall-induced lift force.[40] With the increase in the flow rate, $M > 1$, particles gradually move out from the central focusing stream, and the central focusing stream disappears. When $M \gg 1$, F_{SFD} completely dominates particle movement and particles get trapped in the flow vortices, which is shown as the increase of the stream width for the two side streams.

METHODS

A microchannel was designed for the separation experiments, as shown in Figure 1b. The microchannel has one inlet and three outlets, which correspond to the three particle focusing streams. Fluid is driven by a syringe pump (KDS 200, KD Scientific, Holliston, MA) and passes through the microchannel. The images of focusing streams and cell orientation are observed near the channel outlet region utilizing a

https://doi.org/10.1021/acsomega.2c06021
ACS Omega 2022, 7, 41759−41767

fluorescent microscope (Nikon A1R, Nikon, Japan) and a high-speed imaging system Fastcam Mini UX50 (Photron, San Diego, CA).

PEO was utilized as a polymer additive for viscoelastic fluid. It was obtained from Sigma-Aldrich (St. Louis, MO) with an average molecular weight of 2 MDa. PEO was mixed with a PBS solution to make the polymer solution with the concentration c ranging from 0.1 to 0.5% (wt/v). PEO rheological property was characterized, and all PEO solutions tested in this work can be treated as semidiluted solutions.

Fluorescent polystyrene particles (Polysciences Inc, PA) with diameters of 2, 3, 6, and 10 μm were used to characterize particle focusing in a PEO solution. Blood samples and plasmodium-infected RBCs were prepared for the cell separation experiments in high viscoelastic flow. The experiment was performed with the flow rate ranging from 5 μL/min to 100 μL/min. A detailed description of device fabrication, polymer property characterization, biosample preparation, and experiment setup can be found in the Supporting Information.

RESULTS

Influence of Particle Size. Particle MSF in high viscoelastic flow is highly influenced by the particle dimension, as proposed in eq 3. The experiment has been performed to study size-based cell separation by MSF. Fluorescent beads focusing streams are observed as a reference for the cell separation experiment. The representative image of the transition from single-stream focusing to MSF can be found in the Supporting Information. A color map is created to characterize the particle focusing streams with the change of the flow rate and PEO concentration, as shown in Figure 2. It is found that both the increase in the flow rate and PEO concentration contribute to MSF. Small-sized fluorescent beads start stream bifurcation at a low flow rate and PEO concentration, while the large-sized beads tend to keep the single-stream focusing.

Blood cell focusing in high viscoelastic flow was studied utilizing the same experimental setup. RBCs and WBCs were loaded in the spiral channel device, and the focusing streams color map is demonstrated in Figure 2. RBCs have a single focusing stream in 0.1 and 0.2%wt/v PEO at a low flow rate, and MSF appears with the increase in the flow rate and PEO concentration. The video of the RBC transition from single-stream focusing can be found in the Supporting Information. WBCs have a relatively large size, and they have a single-stream focusing under most of the test conditions.

Separation of RBCs and WBCs can be achieved utilizing the difference in their focusing streams, as shown in Figure 3. RBCs have a volume equivalent sphere diameter of 6 μm, and WBCs have an average diameter of 12 μm.[41] The size difference between RBCs and WBCs contributes to the different focusing positions in the high viscoelastic flow. In low-concentration PEO solution, RBCs have single and transitional focusing streams, which overlap with WBC focusing streams, while in a high-concentration PEO solution, RBCs have MSF. In this case, RBCs and WBCs focus on different positions and can be collected from different outlets. The mixture of RBCs and WBCs is loaded in a 0.5% wt/v PEO solution. At 30 μL/min, RBCs have split focusing streams, while WBCs have a narrow focusing stream in the channel center. It is found that 93.3% of WBCs get focused in the central stream, and 92.5% RBCs are located in side streams.

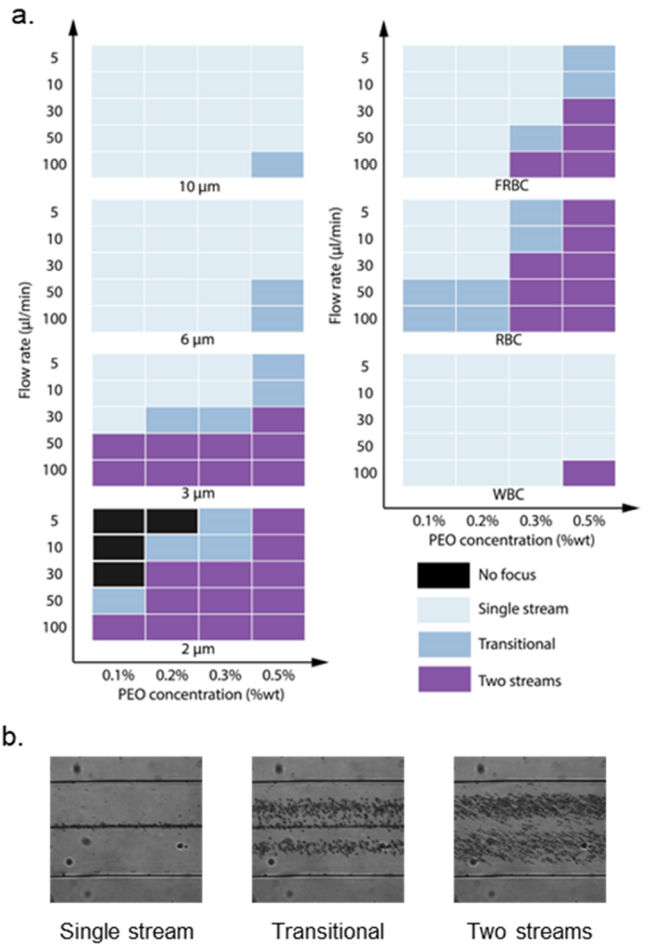

Figure 2. Results of multiple-streams focusing for polystyrene beads and cells. (a) Color map of fluorescent bead and blood cell stream distribution under different flow rates and PEO concentrations. (b) Representative images of particle focusing streams.

Influence of Particle Deformability. The high shear stress in high viscoelastic flow causes cell stretch in the microchannel, which affects cell movement and focusing position. The influence of cell deformability on MSF was studied utilizing RBCs with different deformabilities. When experiencing shear stress, RBCs transform into a prolate ellipsoid shape with a constant surface area.[42] In the experiment, formalin was used for the cross-linking fixation of RBC,[43] which is known to rigidify and thus decrease the deformability of fixed RBCs (FRBC). The focusing streams of FRBC were examined, and the focusing stream color map is shown in Figure 2. FRBCs, with reduced deformability, tend to have a single focusing stream in the channel center. The transition to MSF happens at a higher flow rate and PEO concentration compared to untreated RBCs.

The deformation of RBC was evaluated utilizing a high-speed camera. Figure 4 shows the cell dimension variation of fixed RBCs and normal RBCs in solution with different viscoelastic properties. The maximum disk diameter of RBCs is measured by processing high-speed imaging results in ImageJ to characterize cell stretching in the high viscoelastic flow. In the PEO solution, cells get stretched, leading to an increase in the cell dimension. Under a flow rate of 100 μL/min, the dimensions of normal RBCs increase to 8.78 μm and 12.5 μm diameters in 0.1 and 0.5% wt/v PEO solutions. FRBCs have a

https://doi.org/10.1021/acsomega.2c06021
ACS Omega 2022, 7, 41759−41767

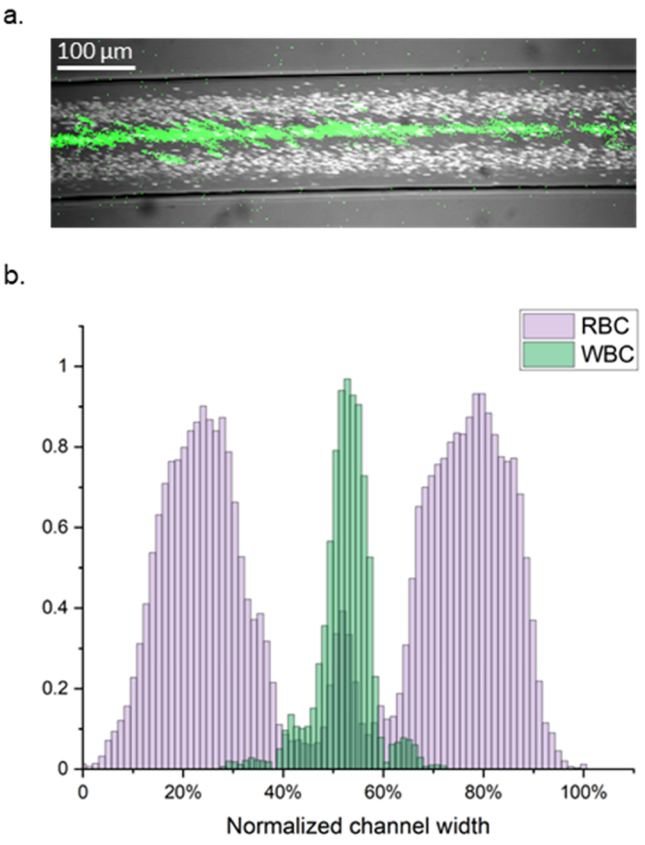

Figure 3. Separation of RBC and WBC in high viscoelastic flow. (a) Image of RBC (white) and WBC (green color) focusing streams in the microchannel. Experiments are performed in the 0.5% wt/v PEO solution at 30 μL/min. (b) Cell concentration intensity of RBC and WBC in the microchannel.

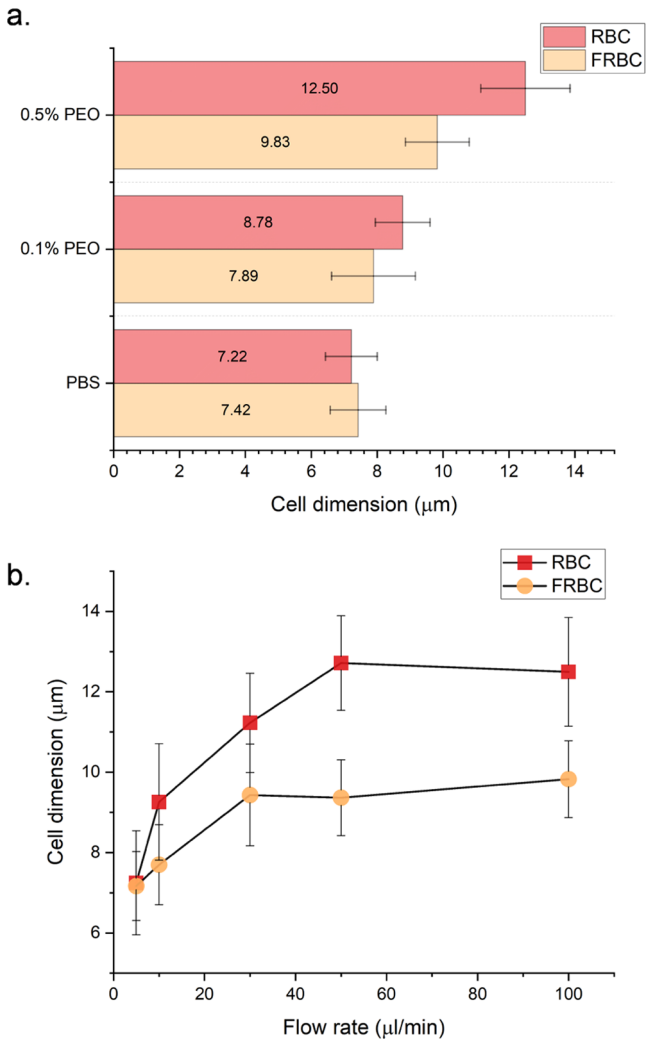

Figure 4. Cell dimension under different flow conditions. (a) Measured cell dimensions of RBC and FRBC in different carrier solutions at a flow rate of 100 μL/min. (b) Measured cell dimensions of RBC and FRBC in the 0.5% PEO solution at different flow rates. Error bars indicate the standard deviation of 200 measurements for each data point.

stiffer surface, and the cell diameter increases up to 9.83 μm in the 0.5% PEO solution. Figure 4b shows the increase in the cell dimension with the increase in the flow rate in the 0.5% wt/v PEO solution. Normal RBCs reach the maximum dimension at 50 μL/min, and FRBCs reach the maximum dimension at 30 μL/min.

The focusing stream distribution of normal RBCs and FRBCs is compared to rigid spherical particles. Figure 5 shows the number of focusing streams in PEO solutions of different concentrations utilizing the data from Figure 2. In this case, the transitional state from the single-stream focusing to two streams focusing is counted as 1.5 focusing streams. RBCs have smaller cell apparent diameters under stretch as they behave like rigid spherical particles with small diameters. Normal RBCs have a focusing stream similar to 3 μm beads in 0.1 and 0.2% PEO solutions, while their focusing stream is similar to 2 μm beads in 0.3 and 0.5% PEO solutions. Fixed RBCs have a single focusing stream in 0.1 and 0.2% PEO, which is similar to 6 μm beads. In a high-concentration PEO solution, fixed RBCs have focusing streams similar to 3 μm beads. As a result, the increase in PEO concentration leads to cell stretching for deformable cells, and the deformed cells behave like smaller spherical-shaped particles.

Influence of Particle Orientation. The presence of viscoelastic secondary flow will affect nonspherical particle rotation and movement in high viscoelasticity flow. The orientation of RBCs in the PEO solution was studied utilizing a high-speed camera. Figure 6a shows the image of RBC movement in a 0.3% wt/v PEO solution at 30 μL/min when RBCs have focusing positions in both the central and side streams. RBCs have different orientations in different focusing streams. In the central focusing stream, RBCs align with the channel height direction, while in the side focusing streams, RBCs align with the channel width direction. Cell orientation change is affected by the dominant force in different focusing positions. In the channel center, cells are focused by the viscoelastic force F_E. The high shear stress is applied from the channel height direction due to the channel cross-section design. When RBCs get focused to split focusing streams near channel side walls, F_{SFD} dominates cell movement, which has orientation in the channel width direction (Figure 6b). The cell stretching is also affected by the particle position and alignment, as RBCs in central focusing stream have smaller diameters compared to RBCs in side streams, where RBCs experience high shear stress (Figure 6c). It is expected that the nonspherical particles have different focusing positions compared to spherical ones due to the interaction between

https://doi.org/10.1021/acsomega.2c06021
ACS Omega 2022, 7, 41759−41767

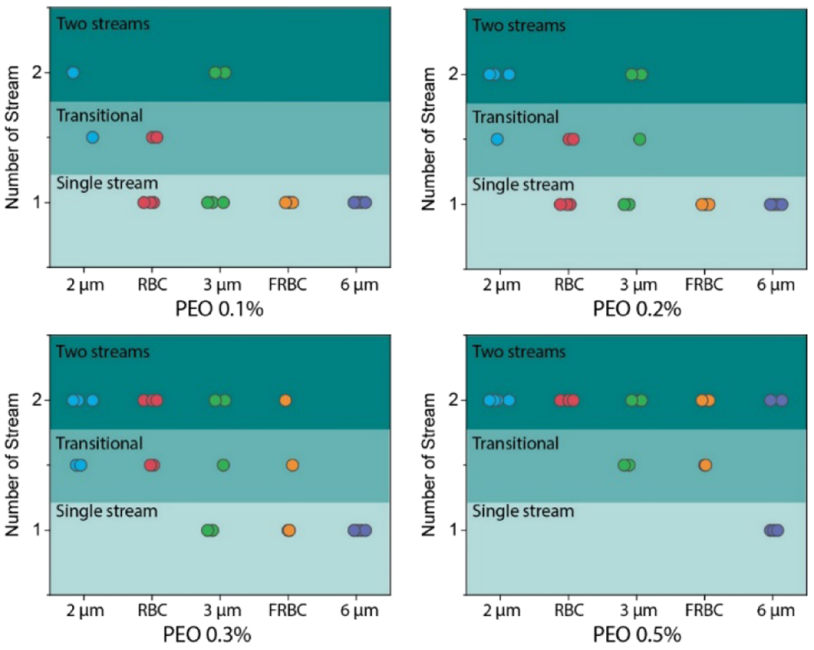

Figure 5. Summary of focusing streams of fluorescent beads, RBC, and FRBC in different PEO solutions.

particle orientation and force distribution, leading to shape-based separation in high viscoelastic flow.

Separation of *Plasmodium*-Infected RBCs from Uninfected RBCs. Severe malaria is caused by *P. falciparum* parasites that invade and grow within red blood cells. During their 48 h development cycle inside RBCs, parasites remodel the host RBC. This parasite-specific remodeling alters the mechanical properties and deformability of the infected RBC and distinguishes it from uninfected RBCs.[44,45] Based on these differences, we hypothesized that MSF in high viscoelastic flow would efficiently separate parasite-infected from uninfected RBCs. Figure 7 shows the distribution of two different *P. falciparum* strains (NF54 and DD2) compared with uninfected RBCs from the hospital blood bank or freshly obtained from donors. It is found that the infected RBCs have a higher propensity to focus in the center of the channel, while the uninfected RBCs are more evenly distributed in all three outlets. The observed change of particle collection from the channel outlets is consistent with expectations that the infected RBC sample, containing predominantly schizont-stage parasites, has higher stiffness compared to uninfected RBCs. In addition, it should be noticed that the blood bank storage RBC has slightly higher distribution in the channel center, which is consistent with the previous report that RBC gets stiffer with extended storage.[46]

The propensity of IRBCs to concentrate in the central channel suggested the possibility of separating a more complex mixture of IRBCs and uninfected RBCs on the basis of MSF. To test the efficiency of such separation, a mixed sample containing 10% schizont-stage infected cells was analyzed on our device. As shown in Figure 8a, it was found that IRBCs preferentially accumulate in the central outlet, while uninfected cells are distributed fairly evenly between the outlets. The separation efficiency of infected from uninfected cells reduces as the flow rate increases, which matches the trend of cell shifts to multiple-streams focusing under a high flow rate observed for fluorescent beads (Figure 2).

The schizont parasitemia in samples collected from each outlet was analyzed by flow cytometry and compared to the input parasitemia of 10%. As shown in Figure 8b, the central outlet sample displayed a twofold increased parasitemia of 20%, while parasitemia in the side outlet samples reduced to 5%. This result confirms the ability of MSF to enrich *Plasmodium*-infected RBCs from a mixture with uninfected RBCs on the basis of differential deformability. Further enrichment might be obtained using a longer flow channel and/or iterative passage of collected streams through the MSF device.

DISCUSSION

Viscoelastic secondary flow-induced MSF is affected by multiple parameters. In our previous study, the influence of fluid property and channel geometry on MSF is explained,[31] as summarized in eq 3. This paper focuses on the influence of cell physical properties in high viscoelastic flow. The microfluidic channel is designed based on previous work with fluorescent beads.[31] With the increase in flow relaxation time, particle focusing in the high viscoelastic flow requires a long channel length.[47] As a result, the serpentine channel design is utilized to increase the channel length, and steady focusing streams are observed with an increased channel length. The PEO solution is selected due to its good biocompatibility and rheology properties.

MSF in high viscoelasticity flow is associated with multiple cell physical properties as cells have different hydrodynamic interactions with such complex flow. Size-based separation, which is widely used in a microfluidic-based separation device, is demonstrated in the high viscoelastic flow. With the increase in particle size, F_E overwhelms F_{SFD} and large particles focus to the channel center, while small particles have MSF. In the blood cell separation experiment, WBCs are efficiently removed from RBCs by forming a narrow stream in the channel center, while the majority of RBCs focus on the side streams. Sheathless size-based separation and enrichment can

https://doi.org/10.1021/acsomega.2c06021
ACS Omega 2022, 7, 41759−41767

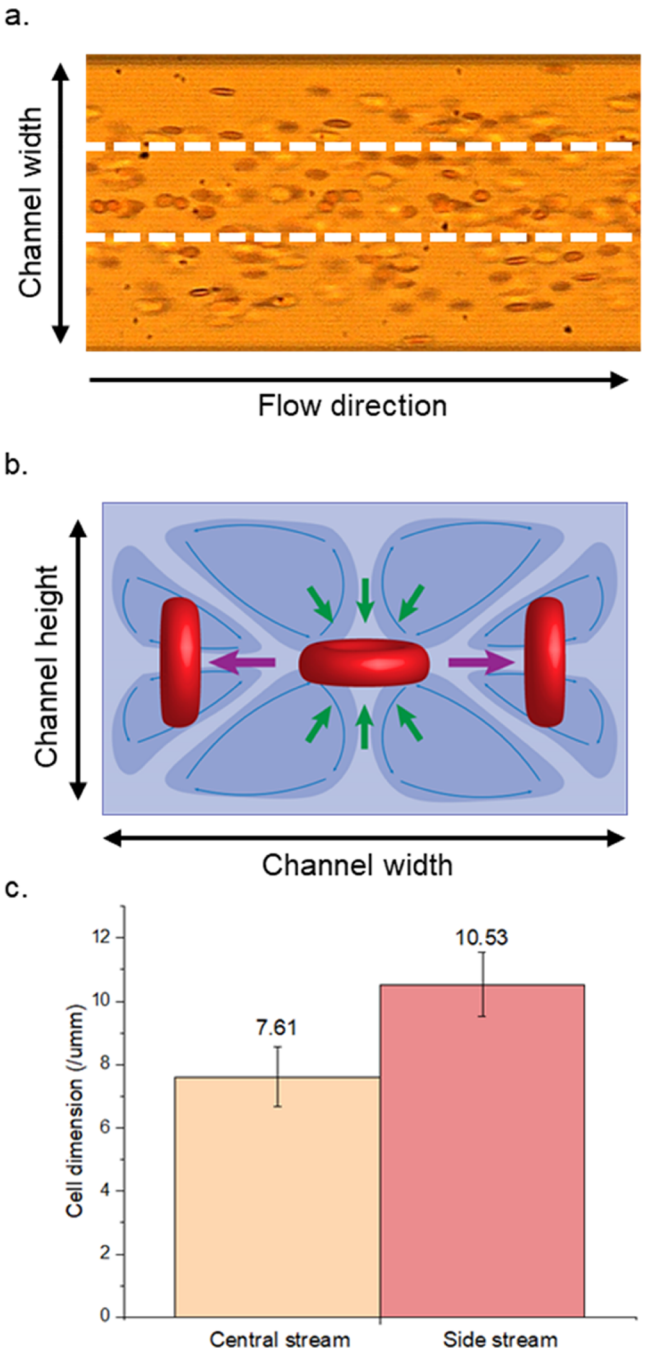

Figure 6. RBC alignment in the multiple-streams focusing condition. (a) Orientation of RBC in central and side streams. The image was taken in the 0.3% PEO solution at 10μl/min. (b) Force distribution-affected cell orientation in different focusing positions. (c) RBC major axial diameter in central focusing stream and side focusing stream. Error bars indicate the standard deviation of 200 measurements for each data point.

be realized based on MSF for high viscoelastic flow-related applications.

Cell mechanical properties are associated with many physiological and pathological processes. Deformability-based particle separation is required in the sample treatment processes such as pathological examination and cell circle synchronization. In Newtonian flow, deformable particle focusing toward the channel center has been verified from experimental results[48] and numerical simulation.[49,50] Viscoe-

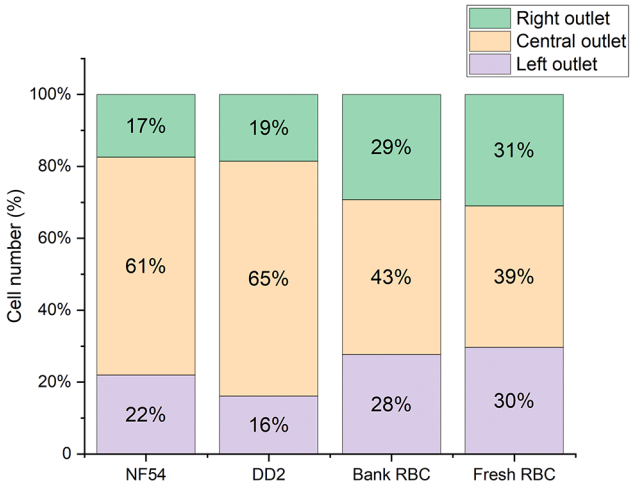

Figure 7. Percentage of IRBC and RBC recovered from the central and side outlets. The experiment was performed using the 0.5% PEO solution at 30 μL/min.

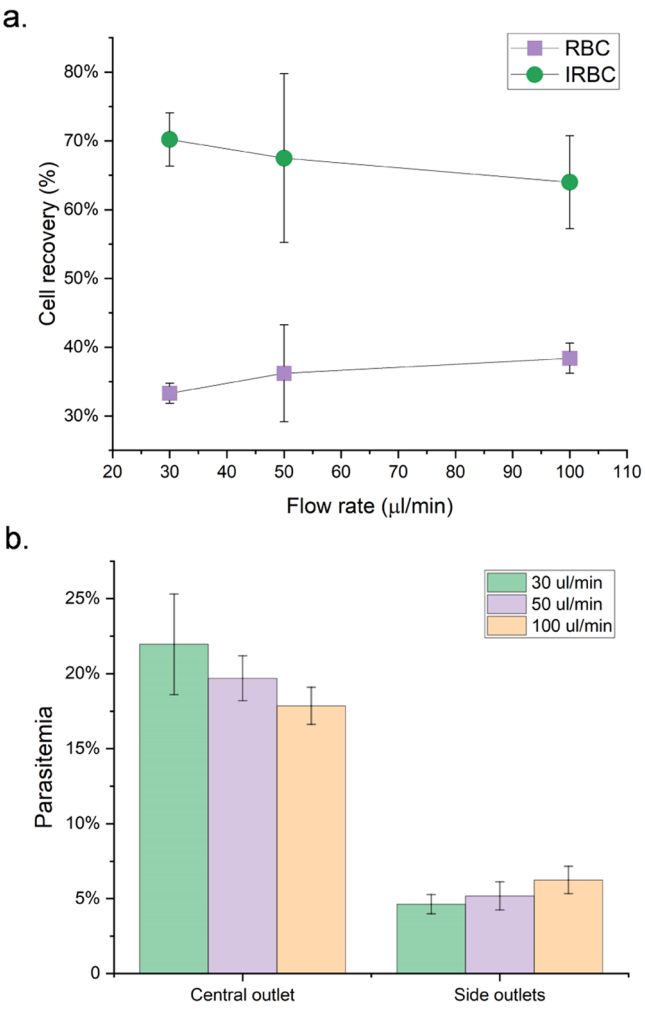

Figure 8. Results of IRBC and RBC separation. (a) Recovery rate of IRBC and RBC from the central stream with the increases in the flow rate. (b) Concentration of IRBC in RBC at different flow rates. The experiment was performed by injecting a 10% starting parasitemia mixture of synchronized IRBCs and RBCs in the microchannel with the 0.5% PEO solution. Error bars indicate the standard deviation of three experiments.

https://doi.org/10.1021/acsomega.2c06021
ACS Omega 2022, 7, 41759−41767

lastic focusing has been used in an extensional flow device for RBC deformability measurement.[51] In high viscoelastic flow, it is observed that deformable cells are more affected by the nonlinear effect and secondary flow. As a result, deformable cells have the tendency to focus in side streams.

The deformability-based separation of IRBCs from RBCs demonstrates the potential of label-free enrichment of parasite-infected RBCs from the blood sample in a simple microfluidic device. In addition to the application in cell separation, the MSF phenomenon provides a new tool for the analysis of physical properties of infectious cells.[52] Continuous, high throughput cell deformability assessment is needed for large-scale cell analysis.[53] The rapid screening of cell deformability can be realized utilizing high viscoelasticity flow cytometry, in which cell mechanical property is evaluated by measuring cell MSF response change under different flow rates in a confined channel.

Nonspherical cells are sensitive to force distribution in a flow field and have different focusing streams compared with spherical particles. In a pressure-driven shear flow, non-spherical particles tend to get aligned with the shear stress field, and particle rotation orbit changes, leading to the change of particle focusing positions.[10,54] Nonspherical cell manipulation and separation in viscoelastic flow have been demonstrated in previous works in which cell focusing positions are controlled by the interaction of different forces, such as the elastoinertial effect,[55] coflow of Newtonian and viscoelastic flow,[56] and Dean flow-coupled viscoelastic flow.[57] The viscoelastic focusing of nonspherical particles mainly depends on the minor axis dimension, and a nonspherical particle has less focusing on the channel center compared to spherical particles with equal volume.[55] In high viscoelastic flow, nonspherical particles experience different forces in different orientations, leading to particle alignment in specific angles. Compared to spherical particles with equivalent volume, nonspherical particles tend to have MSF at a lower flow rate and in low-concentration PEO solutions. Nonspherical particles tend to get aligned with the local shear distribution and secondary flow direction. They experience higher secondary flow drag force as they have a larger projected area when their orientation is vertical to the secondary flow direction.

For deformable RBCs, the cell stretching in high viscoelastic flow leads to the increase of the surface area, which contributes to cell focusing in side streams. The difference in particle shape leads to a change in force distribution. Thus, particles have different balanced positions in the channel cross section due to their shape difference. Further research is necessary to fully understand nonspherical particle alignment and movement in high viscoelastic flow, which contribute to the development of shape-based cell separation approaches utilizing MSF.

CONCLUSIONS

In this work, cell separation in high viscoelastic flow is demonstrated, and the influence of cell physical properties, including cell dimension, deformability, and shape, on cell focusing positions is explored. The N_2-induced viscoelastic secondary flow has a significant influence on cell movement trajectory, and a multiple-streams focusing phenomenon is observed. Size-based cell separation is realized by pushing small cells into side streams while keeping large particles in the channel center. Deformability-based separation is demonstrated for the isolation of *Plasmodium*-infected RBCs from uninfected RBCs, as the high shear stress causes cell stretching. For nonspherical cells such as RBCs, cells exhibit different orientations in different focusing streams due to the coeffect of lift force and drag force. The proposed MSF separation process is passive and label-free, which can be readily utilized in the microscale cell separation process. Particle separation with multiple separation criteria can be realized in the microfluidic device with a simple microchannel design. The proposed separation method has the potential for direct cell separation in biofluids, which are known to have high viscoelasticity, such as saliva, semen, and blood. Such separation methods have potential applications in disease diagnostics and biomarker analysis in clinical samples.

ASSOCIATED CONTENT

Supporting Information

The Supporting Information is available free of charge at https://pubs.acs.org/doi/10.1021/acsomega.2c06021.

Description of the microfluidic chip design and the fabrication process, PEO viscoelasticity measurement, biosample preparation, image acquisition and data processing, viscoelastic flow dimensionless numbers, and test results for beads (PDF)

Transition of focusing streams for RBC (ZIP)

AUTHOR INFORMATION

Corresponding Authors

Haidong Feng − *Department of Mechanical Engineering, University of Utah, Salt Lake City, Utah 84112, United States; Department of Biological Engineering, Massachusetts Institute of Technology, Cambridge, Massachusetts 02139, United States;* orcid.org/0000-0003-1350-4841; Email: fenghd@mit.edu

Bruce K. Gale − *Department of Mechanical Engineering, University of Utah, Salt Lake City, Utah 84112, United States;* orcid.org/0000-0001-5843-3464; Email: bruce.gale@utah.edu

Authors

Dhruv Patel − *Department of Mechanical Engineering, University of Utah, Salt Lake City, Utah 84112, United States*

Jules J. Magda − *Department of Chemical Engineering, University of Utah, Salt Lake City, Utah 84112, United States*

Sage Geher − *Department of Biochemistry, University of Utah School of Medicine, Salt Lake City, Utah 84112, United States*

Paul A. Sigala − *Department of Biochemistry, University of Utah School of Medicine, Salt Lake City, Utah 84112, United States;* orcid.org/0000-0002-3464-3042

Complete contact information is available at: https://pubs.acs.org/10.1021/acsomega.2c06021

Author Contributions

H.F. designed the experiments and wrote the manuscript; D.P. performed high-speed imaging-related experiments; J.M. performed polymer property-related experiments and provided professional guidance; S.G. and P.S. performed malaria-related experiments and provided professional guidance; and B.G. provided funding and project administration.

Notes

The authors declare no competing financial interest.

https://doi.org/10.1021/acsomega.2c06021
ACS Omega 2022, 7, 41759−41767

■ ACKNOWLEDGMENTS

NIH grant (R35GM133764) was given to P.A.S. P.A.S. holds a Career Award at the Scientific Interface from the Burroughs Wellcome Fund and a Pew Biomedical Scholarship from the Pew Charitable Trusts. S.G. was funded in part by a pilot award to P.A.S. from the Utah Center for Iron and Heme Disorders (U54DK110858).

■ REFERENCES

(1) Pamme, N. Continuous flow separations in microfluidic devices. *Lab Chip* **2007**, *7*, 1644−1659.
(2) Sajeesh, P.; Sen, A. K. Particle separation and sorting in microfluidic devices: a review. *Microfluid. Nanofluid.* **2014**, *17*, 1−52.
(3) Carlo, D. D.; Irimia, D.; Tompkins, R. G.; Toner, M. Continuous inertial focusing, ordering, and separation of particles in microchannels. *Proc. Natl. Acad. Sci. U.S.A.* **2007**, *104*, 18892−18897.
(4) Zhou, J.; Papautsky, I. Fundamentals of inertial focusing in microchannels. *Lab Chip* **2013**, *13*, 1121−1132.
(5) Leshansky, A. M.; Bransky, A.; Korin, N.; Dinnar, U. Tunable nonlinear viscoelastic "focusing" in a microfluidic device. *Phys. Rev. Lett.* **2007**, *98*, No. 234501.
(6) D'Avino, G.; Romeo, G.; Villone, M. M.; Greco, F.; Netti, P. A. Single line particle focusing induced by viscoelasticity of the suspending liquid: theory, experiments and simulations to design a micropipe flow-focuser. *Lab Chip* **2012**, 1638.
(7) Xiang, N.; Ni, Z. High-throughput blood cell focusing and plasma isolation using spiral inertial microfluidic devices. *Biomed. Microdevices* **2015**, *17*, 110.
(8) Ozkumur, E.; Shah, A. M.; Ciciliano, J. C.; Emmink, B. L.; Miyamoto, D. T.; Brachtel, E.; Yu, M.; Chen, P.-I.; Morgan, B.; Trautwein, J.; Kimura, A.; Sengupta, S.; Stott, S. L.; Karabacak, N. M.; Barber, T. A.; Walsh, J. R.; Smith, K.; Spuhler, P. S.; Sullivan, J. P.; Lee, R. J.; Ting, D. T.; Luo, X.; Shaw, A. T.; Bardia, A.; Sequist, L. V.; Louis, D. N.; Maheswaran, S.; Kapur, R.; Haber, D. A.; Toner, M. Inertial focusing for tumor antigen-dependent and -independent sorting of rare circulating tumor cells. *Sci. Transl. Med.* **2013**, *5*, 179ra47.
(9) Abdulla, A.; Liu, W.; Gholamipour-Shirazi, A.; Sun, J.; Ding, X. High-Throughput Isolation of Circulating Tumor Cells Using Cascaded Inertial Focusing Microfluidic Channel. *Anal. Chem.* **2018**, *90*, 4397−4405.
(10) Feng, H.; Jafek, A.; Samuel, R.; Hotaling, J.; Jenkins, T.; Aston, K.; Gale, B. High efficiency rare sperm separation from biopsy samples in an inertial focusing device. *Analyst* **2021**, *146*, 3368−3377.
(11) Jafek, A.; Feng, H.; Brady, H.; Petersen, K.; Chaharlang, M.; Aston, K.; Gale, B.; Jenkins, T.; Samuel, R. An automated instrument for intrauterine insemination sperm preparation. *Sci. Rep.* **2020**, *10*, No. 21385.
(12) Di Carlo, D. Inertial microfluidics. *Lab Chip* **2009**, *9*, 3038−3046.
(13) Martel, J. M.; Toner, M. Inertial Focusing in Microfluidics. *Annu. Rev. Biomed. Eng.* **2014**, *16*, 371−396.
(14) Volpe, A.; Gaudiuso, C.; Ancona, A. Sorting of Particles Using Inertial Focusing and Laminar Vortex Technology: A Review. *Micromachines* **2019**, *10*, 594.
(15) Kalyan, S.; Torabi, C.; Khoo, H.; Sung, H. W.; Choi, S.-E.; Wang, W.; Treutler, B.; Kim, D.; Hur, S. C. Inertial Microfluidics Enabling Clinical Research. *Micromachines* **2021**, *12*, 257.
(16) Varchanis, S.; Dimakopoulos, Y.; Wagner, C.; Tsamopoulos, J. How viscoelastic is human blood plasma? *Soft Matter* **2018**, *14*, 4238−4251.
(17) Shi, Y. D.; Pan, L. F.; Yang, F. K.; Wang, S. Q. A preliminary study on the rheological properties of human ejaculate and changes during liquefaction. *Asian J Androl* **2004**, *6*, 299−304.
(18) Kim, B.; Kim, J. M. Elasto-inertial particle focusing under the viscoelastic flow of DNA solution in a square channel. *Biomicrofluidics* **2016**, *10*, 024111.
(19) Kang, K.; Lee, S. S.; Hyun, K.; Lee, S. J.; Kim, J. M. DNA-based highly tunable particle focuser. *Nat. Commun.* **2013**, *4*, No. 2567.
(20) Ho, B. P.; Leal, L. G. Inertial migration of rigid spheres in two-dimensional unidirectional flows. *J. Fluid Mech.* **1974**, *65*, 365−400.
(21) Yang, S.; Kim, J. Y.; Lee, S. J.; Lee, S. S.; Kim, J. M. Sheathless elasto-inertial particle focusing and continuous separation in a straight rectangular microchannel. *Lab Chip* **2011**, *11*, 266−273.
(22) Liu, C.; Xue, C.; Chen, X.; Shan, L.; Tian, Y.; Hu, G. Size-Based Separation of Particles and Cells Utilizing Viscoelastic Effects in Straight Microchannels. *Anal. Chem.* **2015**, *87*, 6041−6048.
(23) Li, D.; Lu, X.; Xuan, X. Viscoelastic separation of particles by size in straight rectangular microchannels: a parametric study for a refined understanding. *Anal. Chem.* **2016**, *88*, 12303−12309.
(24) Nam, J.; Lim, H.; Kim, D.; Jung, H.; Shin, S. Continuous separation of microparticles in a microfluidic channel via the elasto-inertial effect of non-Newtonian fluid. *Lab Chip* **2012**, *12*, 1347−1354.
(25) Yuan, D.; Zhang, J.; Yan, S.; Pan, C.; Alici, G.; Nguyen, N. T.; Li, W. H. Dean-flow-coupled elasto-inertial three-dimensional particle focusing under viscoelastic flow in a straight channel with asymmetrical expansion-contraction cavity arrays. *Biomicrofluidics* **2015**, *9*, 044108.
(26) Tian, F.; Zhang, W.; Cai, L.; Li, S.; Hu, G.; Cong, Y.; Liu, C.; Li, T.; Sun, J. Microfluidic co-flow of Newtonian and viscoelastic fluids for high-resolution separation of microparticles. *Lab Chip* **2017**, *17*, 3078−3085.
(27) Hazra, S.; Jayaprakash, K. S.; Pandian, K.; Raj, A.; Mitra, S. K.; Sen, A. K. Non-inertial lift induced migration for label-free sorting of cells in a co-flowing aqueous two-phase system. *Analyst* **2019**, *144*, 2574−2583.
(28) Yuan, D.; Zhao, Q.; Yan, S.; Tang, S.-Y.; Alici, G.; Zhang, J.; Li, W. Recent progress of particle migration in viscoelastic fluids. *Lab Chip* **2018**, *18*, 551−567.
(29) Lim, H.; Nam, J.; Shin, S. Lateral migration of particles suspended in viscoelastic fluids in a microchannel flow. *Microfluid. Nanofluid.* **2014**, *17*, 683−692.
(30) Villone, M. M.; D'Avino, G.; Hulsen, M. A.; Greco, F.; Maffettone, P. L. Particle motion in square channel flow of a viscoelastic liquid: Migration vs. secondary flows. *J. Non-Newtonian Fluid Mech.* **2013**, *195*, 1−8.
(31) Feng, H.; Magda, J. J.; Gale, B. K. Viscoelastic second normal stress difference dominated multiple-stream particle focusing in microfluidic channels. *Appl. Phys. Lett.* **2019**, *115*, No. 263702.
(32) Feng, H.; Jafek, A. R.; Wang, B.; Brady, H.; Magda, J. J.; Gale, B. K. Viscoelastic Particle Focusing and Separation in a Spiral Channel. *Micromachines* **2022**, *13*, No. 361.
(33) Xiang, N.; Zhang, X.; Dai, Q.; Cheng, J.; Chen, K.; Ni, Z. Fundamentals of elasto-inertial particle focusing in curved microfluidic channels. *Lab Chip* **2016**, *16*, 2626−2635.
(34) Zhou, J.; Papautsky, I. Viscoelastic microfluidics: progress and challenges. *Microsyst. Nanoeng.* **2020**, *6*, 113.
(35) Larson, R. G.*The Structure and Rheology of Complex Fluids*; Oxford University Press, 1998; p 688.
(36) Magda, J. J.; Baek, S. G. Concentrated entangled and semidilute entangled polystyrene solutions and the second normal stress difference. *Polymer* **1994**, *35*, 1187−1194.
(37) Debbaut, B.; Avalosse, T.; Dooley, J.; Hughes, K. On the development of secondary motions in straight channels induced by the second normal stress difference: experiments and simulations. *J. Non-Newtonian Fluid Mech.* **1997**, *69*, 255−271.
(38) Xue, S. C.; Phan-Thien, N.; Tanner, R. I. Numerical study of secondary flows of viscoelastic fluid in straight pipes by an implicit finite volume method. *J. Non-Newtonian Fluid Mech.* **1995**, *59*, 191−213.
(39) Yue, P.; Dooley, J.; Feng, J. J. A general criterion for viscoelastic secondary flow in pipes of noncircular cross section. *J. Rheol.* **2008**, *52*, 315−332.
(40) Abkarian, M.; Viallat, A. Dynamics of Vesicles in a Wall-Bounded Shear Flow. *Biophys. J.* **2005**, *89*, 1055−1066.

https://doi.org/10.1021/acsomega.2c06021
ACS Omega 2022, 7, 41759−41767

(41) Prinyakupt, J.; Pluempitiwiriyawej, C. Segmentation of white blood cells and comparison of cell morphology by linear and naïve Bayes classifiers. *Biomed. Eng. Online* **2015**, *14*, No. 63.
(42) Fischer, T. M.; Stöhr-Liesen, M.; Schmid-Schönbein, H. The Red Cell as a Fluid Droplet: Tank Tread-Like Motion of the Human Erythrocyte Membrane in Shear Flow. *Science* **1978**, *202*, 894−896.
(43) Thavarajah, R.; Mudimbaimannar, V. K.; Elizabeth, J.; Rao, U. K.; Ranganathan, K. Chemical and physical basics of routine formaldehyde fixation. *J. Oral Maxillofac. Pathol.* **2012**, *16*, 400−405.
(44) Suwanarusk, R.; Cooke, B. M.; Dondorp, A. M.; Silamut, K.; Sattabongkot, J.; White, N. J.; Udomsangpetch, R. The Deformability of Red Blood Cells Parasitized by *Plasmodium falciparum* and P. vivax. *J. Infect. Dis.* **2004**, *189*, 190−194.
(45) Herricks, T.; Antia, M.; Rathod, P. K. Deformability limits of *Plasmodium falciparum*-infected red blood cells. *Cell. Microbiol.* **2009**, *11*, 1340−1353.
(46) Frank, S. M.; Abazyan, B.; Ono, M.; Hogue, C. W.; Cohen, D. B.; Berkowitz, D. E.; Ness, P. M.; Barodka, V. M. Decreased Erythrocyte Deformability After Transfusion and the Effects of Erythrocyte Storage Duration. *Anesth. Analg.* **2013**, *116*, 975−981.
(47) Li, Z.; Haward, S. J. Viscoelastic flow development in planar microchannels. *Microfluid. Nanofluid.* **2015**, *19*, 1123−1137.
(48) Reichel, F.; Mauer, J.; Nawaz, A. A.; Gompper, G.; Guck, J.; Fedosov, D. A. High-Throughput Microfluidic Characterization of Erythrocyte Shapes and Mechanical Variability. *Biophys. J.* **2019**, *117*, 14−24.
(49) Alghalibi, D.; Rosti, M. E.; Brandt, L. Inertial migration of a deformable particle in pipe flow. *Phys. Rev. Fluids* **2019**, *4*, 104201.
(50) Rezghi, A.; Li, P.; Zhang, J. Lateral migration of viscoelastic capsules in tube flow. *Phys. Fluids* **2022**, *34*, 011906.
(51) Cha, S.; Shin, T.; Lee, S. S.; Shim, W.; Lee, G.; Lee, S. J.; Kim, Y.; Kim, J. M. Cell Stretching Measurement Utilizing Viscoelastic Particle Focusing. *Anal. Chem.* **2012**, *84*, 10471−10477.
(52) Ito, H.; Kaneko, M. On-chip cell manipulation and applications to deformability measurements. *ROBOMECH J.* **2020**, *7*, No. 3.
(53) Fregin, B.; Czerwinski, F.; Biedenweg, D.; Girardo, S.; Gross, S.; Aurich, K.; Otto, O. High-throughput single-cell rheology in complex samples by dynamic real-time deformability cytometry. *Nat. Commun.* **2019**, *10*, No. 415.
(54) Prohm, C.; Zöller, N.; Stark, H. Controlling inertial focussing using rotational motion. *Eur. Phys. J. E* **2014**, *37*, 36.
(55) Lu, X.; Xuan, X. Elasto-Inertial Pinched Flow Fractionation for Continuous Shape-Based Particle Separation. *Anal. Chem.* **2015**, *87*, 11523−11530.
(56) Liu, P.; Liu, H.; Yuan, D.; Jang, D.; Yan, S.; Li, M. Separation and Enrichment of Yeast Saccharomyces cerevisiae by Shape Using Viscoelastic Microfluidics. *Anal. Chem.* **2021**, *93*, 1586−1595.
(57) Yuan, D.; Yan, S.; Zhang, J.; Guijt, R. M.; Zhao, Q.; Li, W. Sheathless Separation of Cyanobacterial Anabaena by Shape Using Viscoelastic Microfluidics. *Anal. Chem.* **2021**, *93*, 12648−12654.

https://doi.org/10.1021/acsomega.2c06021
ACS Omega 2022, 7, 41759−41767